



## SENSING CHARACTERISTICS OF ZnO NANOPARTICLE FILM TOWARDS ACETONE

Dinesh Kumar Chaudhary<sup>1,2</sup>, Yogesh Singh Maharjan<sup>1</sup>, Sharmila Pradhan Amatya<sup>3</sup>, Shankar Prasad Shrestha<sup>4</sup>, Rajendra Parajuli<sup>1</sup>, Pitamber Shrestha<sup>1</sup>, Leela Pradhan Joshi<sup>1\*</sup>

<sup>1</sup>Physics Department, Amrit Campus, Tribhuvan University, Kathmandu, Nepal

<sup>2</sup>Central Department of Physics, Tribhuvan University, Kirtipur, Kathmandu, Nepal

<sup>3</sup>Chemistry Department, Amrit Campus, Tribhuvan University, Kathmandu, Nepal

<sup>4</sup>Physics Department, Patan Multiple Campus, Lalitpur, Nepal

Corresponding Author: [leela.pradhanjoshi@ac.tu.edu.np](mailto:leela.pradhanjoshi@ac.tu.edu.np)

(Received: November 16, 2021; Revised: May 16, 2022; Accepted: June 30, 2022)

### ABSTRACT

Over the past few decades, nanomaterials of metal oxide such as zinc oxide (ZnO) have been significantly researched for sensing various toxic gases like ethanol, acetone and ammonia. The sensing performance of semiconducting materials depends primarily on their surface structure and the interaction behavior with target gas molecules. The surface quality of ZnO is highly influenced by deposition methods. Although several ZnO surfaces have been rigorously studied for detecting gas leakages, it still possesses drawbacks such as high operating temperature, slow response and recovery times. Henceforth, this investigation was carried out to resolve these issues in the fabrication of future ZnO-based gas sensors. In this work, we report the major findings of the ZnO-based nanoparticle film gas sensor prepared by a doctor blade method to gain insight towards detecting various concentrations of acetone gas at different temperatures. The XRD and FTIR results confirmed the phase purity of ZnO. The results showed the highest response ratio of  $25.697 \pm 0.012$  at 285 °C with an exposure of 800 ppm of acetone along with the quick response and recovery times of 39 sec and 79 sec, respectively. This operating temperature was found to be lower than the reported value for a similar system than that prepared via different methods.

**Keywords:** Acetone sensor, Operating temperature, Response time, ZnO nanoparticle

### INTRODUCTION

Acetone is one of the most common but toxic gases ubiquitously used at many workplaces that include research laboratories, hospitals and chemical manufacturing plants which require immediate attention for its safe remediation. Acetone is also used as an effective biomarker in the diagnosis of type I diabetes. Acetone concentration in a healthy individual should be below 0.8 ppm, while for a diabetic patient it is above 1.8 ppm (Drmosh *et al.*, 2021; Qiang *et al.*, 2016). Exposure to acetone can cause severe damage to the liver, lungs, kidney and central nervous system (Li *et al.*, 2014). Therefore, it is immensely important to understand and develop effective devices to detect even the low traces of acetone (Kishore *et al.*, 2021). Nanomaterials of various metal oxides such as ZnO, Mn-ZnO, Fe<sub>2</sub>O<sub>3</sub>, ZnO-SnO<sub>2</sub>, Au/Ag/Cu doped ZnO, ZnO-TiO<sub>2</sub>, etc., have been widely studied to detect toxic and flammable gases because of its interesting electrical, optical and structural properties (Chen *et al.*, 2017; Qi *et al.*, 2008; Zhu *et al.*, 2017). The sensing performance of metal oxide semiconductors is highly dependent on their surface morphology and interfacial structures. ZnO can be prepared using a number of methods such as sol-gel route, electro-spinning and hydrothermal route, phase transport method, solvothermal method etc., (Kashout *et al.*, 2010; Cui *et al.*, 2016; Hosseini *et al.*, 2015; Xiao *et al.*, 2012). Various efforts have been made to improve gas sensitivity, response and recovery time, reaction rate as well as stability of the ZnO gas sensor. However, these sensors greatly suffer from the inherent drawback of a

high operating temperature of more than 300 °C (Xiao *et al.*, 2012; Chu *et al.*, 2012; Al-Hadeethi *et al.*, 2017; Wongrat *et al.*, 2017). So, it is essential to develop a low cost but effective gas sensor with enhanced sensing performance at lower operating temperatures. To date, ZnO films of various morphologies including nanoparticles, nano rods, nano wires, nano belts, nano sheets and nano fibers have been fabricated (Zhang *et al.*, 2018; Zeng *et al.*, 2009; Zhang *et al.*, 2012; Xi *et al.*, 2007; Wang *et al.*, 2020; Samanta *et al.*, 2015). Among these, ZnO nanoparticles (ZnO NPs) are regarded as a promising metal oxide nanostructures to their large surface area, high chemical, thermal stability, and high yield (Zhao *et al.*, 2019; Bhatia *et al.*, 2017; Tang *et al.*, 2007).

This work reports the fabrication of a chemical sensor based on ZnO NPs to detect as various concentrations of acetone vapors as possible with improved response ratio, response time and recovery time at operating temperature that is lower than reported values.

### EXPERIMENT

#### Chemicals

Zinc acetate dehydrated, ethanol, sodium hydroxide, stannous chloride dehydrated, concentrated hydrochloric acid were purchased from merk and used without further modifications. Distilled water was used throughout the experiment to prepare the ZnO NPs and their film.

### Preparation of ZnO films via doctor blade method

At first, fluorine doped tin oxide layers were deposited on clean glass substrate using the spray pyrolysis method. The prepared layers were found to be transparent and conducting. After then, ZnO films were deposited on these FTO substrates using the paste of ZnO NPs with ethanol and few drops of vinegar as a binder followed by annealing at 550°C for an hour. The prepared film was further aged at room temperature for 7 days to improve the stability before testing (Zhang *et al.*, 2018). Prior to this the ZnO NPs were prepared by reacting the alcoholic solution of zinc acetate with sodium hydroxide via the precipitation method. The residue obtained here were centrifuged at 2500 rpm and filtered very carefully followed by several times washing with distilled water and ethanol to remove organic impurities and dried at a temperature of 550°C inside a programmable muffle furnace (Nabertherm GmbH, LT 3/11/B4 10 Serial No. 36140, Germany) for an hour (Joshi *et al.*, 2021).

The structural investigation of ZnO NPs was completed using X-ray diffractometer (Bruker AXS, D2PHASER A26-X1-A2BOB2A-, Serial No: 207047) with CuK $\alpha$  radiation of wavelength 1.54056 Å. The sensitivity was measured in terms of electrical resistance change before and after gas exposure that was measured using a high-quality digital fluke multimeter in the temperature range of 100–330°C. The base temperature of the chamber was maintained at 150 °C to convert from liquid to vapour phase. The sensor performance of the prepared ZnO NPs film was calculated by taking the resistance ratio,  $Response, R = \frac{R_a}{R_g}$  or  $Sensitivity, S \% = \left(\frac{R_a - R_g}{R_a}\right) \times 100$  where  $R_a$  and  $R_g$  are the resistances of the sensing element (ZnO) in the air and gas respectively (Chu *et al.*, 2012).

## RESULTS AND DISCUSSION

### Structural investigation

The structural properties of as-prepared ZnO NPs were investigated by analyzing its X-ray diffraction pattern. Figure 1(a) depicts the XRD pattern of ZnO using CuK $\alpha$  radiation of wavelength 1.54056 Å in the 2 $\theta$  range of 20°–85°. Measuring peak position (2 $\theta$ ) and corresponding full width half maximum ( $\beta$ ), the crystallite size (D) of ZnO was calculated using Debye Scherer's formula,  $D = \frac{0.94\lambda}{\beta \cos\theta}$  where 0.94 is the correction factor (Bhatia *et al.*, 2017). The observed peaks obtained at 2 $\theta$  = 31.0618, 33.7285, 35.5518, 46.8524, 55.9166, 62.1954, 65.7034, 67.2904, 68.4153, 71.8966, 76.3435 and 80.6931° were indexed as (100), (002), (101), (102), (110), (103), (200), (112), (201), (004), (202) and (104) planes. These observed peaks were indexed with reference to standard JCPDS d-spacing values of pdf # 36-1451 (Al-Hardan *et al.*, 2013; Prajapati *et al.*, 2013). The multiple sharp peaks ascertained the polycrystalline nature of ZnO. Considering all the peak values, we calculated the average crystallite size of ZnO which was found to be 20.77  $\pm$  0.90 nm. The details of the calculation of average D were shown in table 1. The c/a ratio was found as 1.60 suggested the wurtzite hexagonal phase of ZnO. The average microstrain (4 $\eta$ ) and crystallite size (D) were also calculated from the slope of  $\beta \cos\theta$  against  $\sin\theta$  plot (Figure 1(b)) and Williamson-Hall equation,  $\beta \cos\theta = \frac{k\lambda}{D} + 4\eta \sin\theta$  (Hassan *et al.*, 2014). The value of microstrain was found to be 0.0025  $\pm$  0.0012. Using the intercept value, the D was calculated as 24.38  $\pm$  2.16 nm. The absence of impurity phases in the XRD confirmed the purity of prepared material.

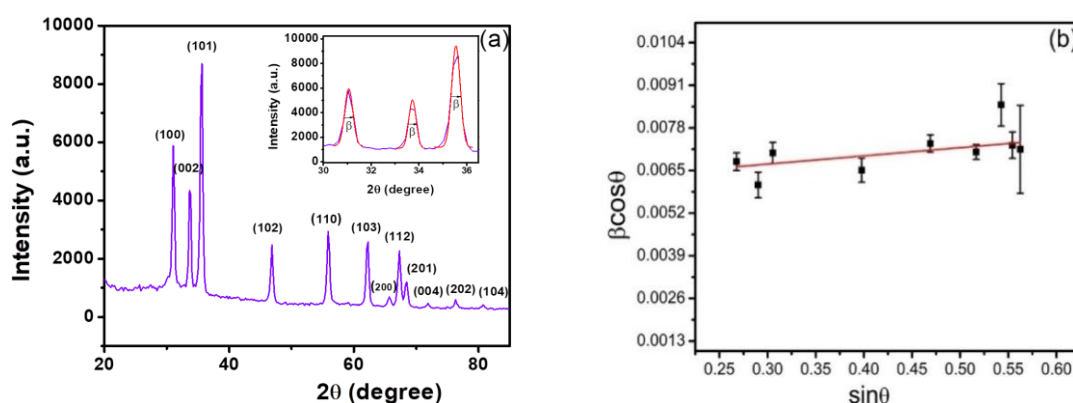


Figure 1. (a) X-ray diffraction pattern (Inset: Determination of  $\beta$ ) and (b) W-H plot of as-prepared ZnO NPs

**Table 1. Observed 2 $\theta$ , FWHM, d-spacings and crystallite size (D) of ZnO**

(hkl)	2 $\theta$ (degree)	FWHM (degree)	d- spacing (Å)	d-spacing (Å) JCPDS	D (nm)	Average D (nm)
(100)	31.0618	0.4027	2.8756	2.8143	21.38	
(002)	33.7285	0.3627	2.6541	2.6033	23.89	
(101)	35.5518	0.4232	2.5221	2.4759	20.57	
(102)	46.8524	0.4062	1.9367	1.9111	22.25	
(110)	55.9166	0.4748	1.6424	1.6247	19.78	20.77 $\pm$ 0.90
(103)	62.1954	0.4726	1.4908	1.4771	20.48	
(200)	65.7034	0.5796	1.4194	1.4071	17.03	
(112)	67.2904	0.5002	1.3898	1.3781	19.91	
(201)	68.4153	0.4949	1.3696	1.3582	20.27	
(004)	71.8966	0.4096	1.3116	1.3017	25.02	
(202)	76.3143	0.4277	1.2463	1.2380	24.67	
(104)	80.6983	0.7809	1.1893	1.1816	13.94	

### Fourier Transform Infrared Analysis

The bond identification of investigated material was done using a Perkin Elmer -16.10.2 FTIR spectrum version in the range 400 to 4000  $\text{cm}^{-1}$ , ATR mode. Fig. 2 shows the FTIR spectrum of so-prepared ZnO NPs

which clearly show a large well defined characteristic peak at 524, followed by small peaks at 685, and 872  $\text{cm}^{-1}$  due to Zn-O stretching (Sirdeshpande *et al.*, 2018). Weak peak observed at 3489  $\text{cm}^{-1}$  attributes for the OH stretching mode of surface hydroxyl groups.

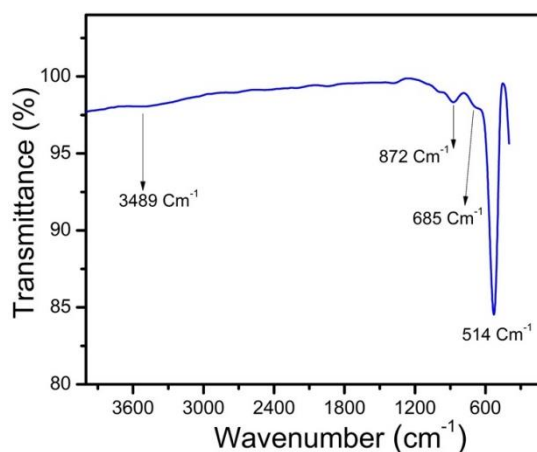


**Figure 2. FTIR spectrum of as-prepared ZnO NPs**

### Sensing Characteristics

The sensing behavior of as-prepared ZnO NPs film towards acetone vapour was investigated in the various temperatures. The ratio of  $R_a$  (resistance in the air) and  $R_g$  (the resistance in gas) gives the sensor performance. The sensor performance of ZnO depends on the reaction rate of test gas with surface adsorbed oxygen species such as  $\text{O}^-$ ,  $\text{O}_2^-$  and  $\text{O}_2^-$ , that depends on its temperature (Chaudhary *et al.*, 2020, Xu *et al.*, 2015). Hence, to optimize the working temperature, the response characteristics were measured in the temperature range of 100-310  $^\circ\text{C}$  with an exposure of 800 ppm of acetone. Figure 3(a) showed the measured sensor characteristics at different temperatures. It shows that the highest value of response ratio, 26 at 285 $^\circ\text{C}$ . The increase of response ratio with temperature is shown in Figure 3(b). The graph also showed a low response at low temperatures which was attributed to the low

reaction rate between the acetone gas molecules with the surface adsorbed oxygen species and high activation energy (Hongstith *et al.*, 2010). The enhancement of the sensor response on increasing the operating temperature was due to the increase in thermal energy to overcome the activation energy. Above optimum temperature, desorption of oxygen molecules occurs from the ZnO surface that may ascribe to decrease the gas response (Khayatyan *et al.*, 2014).

In the gas sensor, response and recovery times are considered as the two important parameters to be known well. The time required to achieve the 90% and 10% of maximum response after injecting and ejecting the test gas are called response and recovery time respectively. Since the carrier concentration of metal oxide semiconductor is a temperature dependent quantity, the response and recovery times are also temperature

dependent. The inset of figure 3(b) shows the graphical calculation of response and recovery times measured with 800 ppm exposure of acetone at 285°C. Figure 3(c) showed that response curves measured with exposure of various concentrations of acetone. The details of calculated response ratio, response and recovery times at 285°C with different concentrations (40-800 ppm) of

acetone were shown in table 2. The inset of this figure clearly showed the linear increase of gas response with the concentration of acetone. Figure 3(d) illustrates measured response curves for three cycles with an exposure of 800 ppm of acetone at 285 °C. The result obviously showed good stability of the ZnO sensor.

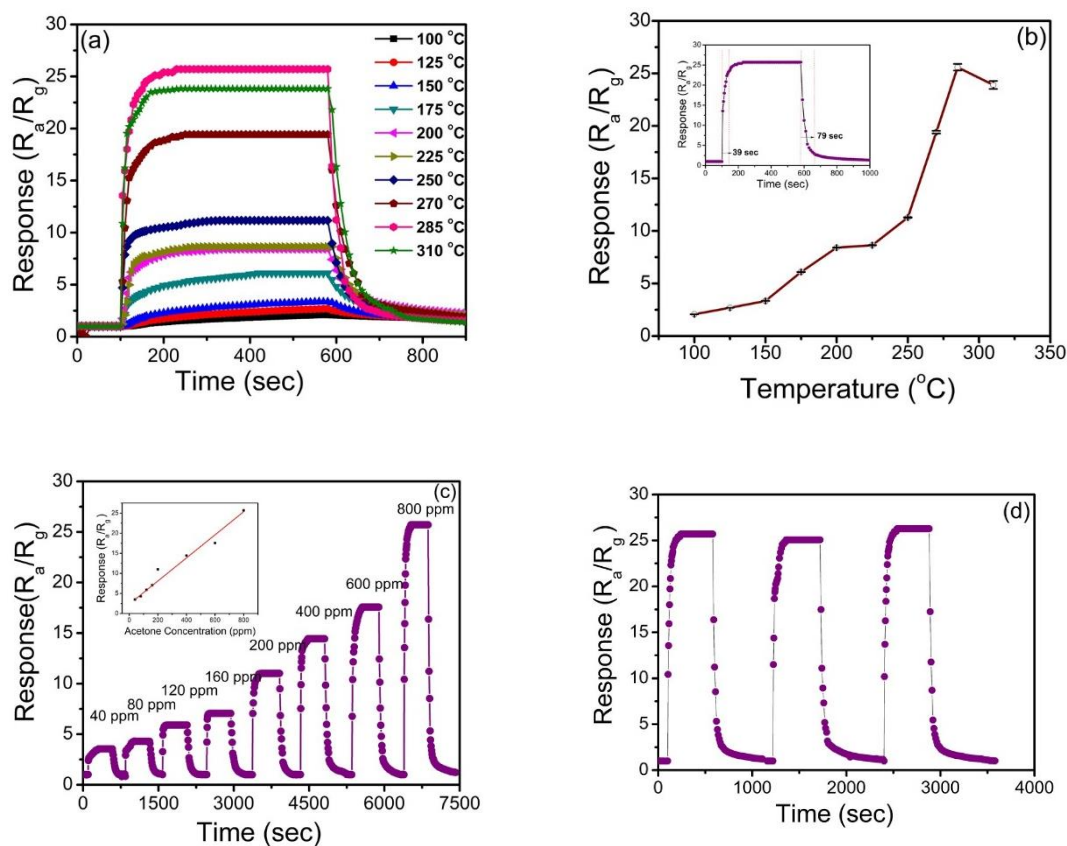


**Figure 3.** (a) Transient response characteristics at various temperatures (b) Temperature dependent response [inset: response and recovery times at 800 ppm acetone] (c) Response curves at different ppm of acetone [inset: increasing gas response with ppm of acetone] (d) stability curves at 800 ppm

The highest gas response with the higher concentration can be seen clearly which was due to the increase in the surface coverage of acetone molecules on the film that enhanced the interaction rate of gas molecules with the adsorbed oxygen species. The result also showed the changes in response and recovery times with the concentration of acetone. The result showed the

response and recovery times for 800 ppm at 285°C were 39 sec and 79 sec respectively. These values were compared with some reported values shown in table 3 for analogous systems but prepared by different methods such as solvothermal, hydrothermal, spray pyrolysis and electro spinning etc.

**Table 2. Response ratio, response and recovery times at different concentrations of acetone at 285 °C**

Concentration (ppm)	Response ( $R_a/R_g$ )	Response time (sec)	Recovery time (sec)
40	$3.500 \pm 0.002$	21	91
80	$4.299 \pm 0.002$	23	101
120	$5.899 \pm 0.003$	21	99
160	$7.052 \pm 0.003$	22	100
200	$11.009 \pm 0.006$	26	95
400	$14.430 \pm 0.007$	28	97
600	$17.562 \pm 0.008$	31	88
800	$25.697 \pm 0.012$	39	79

**Table 3. Comparison of operating temperature, response ratio, response and recovery times with reported works**

Sample	Method	Conc. (ppm)	Operating Temperature (°C)	Response/Sensitivity %	Res/Rec time (sec)	Reference
ZnO nanosheets	Solvothermal	500	420	70	NR	Xiao <i>et al.</i> , 2012
La-ZnO	Solvothermal	1000	385 425	1800 1826	16/3 sec	Chu <i>et al.</i> , 2012
Ag-ZnO Needle	Facile Hydrothermal	200	370	30.233	10/21	Al-Hadeethi <i>et al.</i> , 2017
Pt-ZnO	Thermal Oxidation	400	400	188	NR	Wongrat <i>et al.</i> , 2017
ZnO NPs	Chemical	100	370	36	12/14	Zhang <i>et al.</i> , 2017
Pd-ZnO NPs	Solution		340	76	8/10	
Cr-ZnO	RF co-sputtering	500	400 300	90	210/70 170/95	Al-Hardan <i>et al.</i> , 2013
In-ZnO	Spray Pyrolysis	100	300	96.8	65/24	Prajapati <i>et al.</i> , 2014
La-ZnO	Electro Spinning	200	340	68	2/23	Xu <i>et al.</i> , 2015
ZnO NPs	Precipitation	800 40	285	26 3.5	39/79 21/91	This work.

## CONCLUSIONS

ZnO NPs prepared by the precipitation method were used for the gas sensing task. The XRD results confirmed the polycrystalline ZnO phase with an average crystallite size of  $20.77 \pm 0.90$  nm. Additionally, the chemical bonding of ZnO was studied using the FTIR spectrum. Various concentrations of acetone were tested using ZnO NPs films in temperatures ranging from 100 to 310 °C. The film showed the low and slow response and recovery at low temperatures and high and fast response at higher temperatures. The film showed the highest response of  $25.697 \pm 0.012$  for 800 ppm of acetone vapors at 285 °C with response and recovery time of 39 s and 79 s. The gas sensing results on the exposure of the different concentrations (40-800 ppm) of acetone vapour showed the higher response with an exposure of high concentrations. The highest and lowest values of gas response were found to be  $\sim 26$  for 800 ppm and  $\sim 3.5$  for 40 ppm of acetone.

## ACKNOWLEDGMENTS

We would like to thank the International Science Program (ISP), Uppsala University, Sweden, under NEP-01 grant for providing financial support for chemicals and design & constructing sensor setup.

## AUTHOR CONTRIBUTIONS

Conceptualization, experimental design, data collection and analysis and manuscript preparation were initiated by DKC and LPJ. The FTIR analysis was performed by SPA. YMS, SPS, RP and PS contributed in the data analysis, manuscript writing, review and proof reading.

## CONFLICTS OF INTEREST

The authors declare that they have no competing interests.

## DATA AVAILABILITY STATEMENT

The data that support the findings of this study are available from the corresponding author, upon reasonable request.

## REFERENCES

- Al-Hadeethi, Y., Umar, A., Ibrahim, A. A., Al-Heniti, S. H., Kumar, R., Baskoutas, S., & Raffah, B. M. (2017). Synthesis, characterization and acetone gas sensing applications of Ag-doped ZnO nanoneedles. *Ceramics International*, *43*(9), 6765-6770.
- Al-Hardan, N. H., Abdullah, M. J., & Aziz, A. A. (2013). Performance of Cr-doped ZnO for acetone sensing. *Applied surface science*, *270*, 480-485.
- Bhatia, S., Verma, N., & Bedi, R. K. (2017). Ethanol gas sensor based upon ZnO nanoparticles prepared by different techniques. *Results in Physics*, *7*, 801-806.
- Chaudhary, D. K., Ghimire, R., Amatya, S. P., Shrestha, S. P., & Joshi, L. P. (2020, December). Study on influence of Fe doping into ZnO film for ethanol sensing. *Journal of Physics: Conference Series* (Vol. 1706, No. 1, p. 012036). IOP Publishing.
- Chen, N., Li, Y., Deng, D., Liu, X., Xing, X., Xiao, X., & Wang, Y. (2017). Acetone sensing performances based on nanoporous TiO<sub>2</sub> synthesized by a facile hydrothermal method. *Sensors and Actuators B: Chemical*, *238*, 491-500.
- Chu, X., Zhu, X., Dong, Y., Ge, X., Zhang, S., & Sun, W. (2012). Acetone Sensors Based on La<sup>3+</sup> doped ZnO nano-rods prepared by solvothermal method. *Journal of Materials Science & Technology*, *28*(3), 200-204.
- Cui, J., Shi, L., Xie, T., Wang, D., & Lin, Y. (2016). UV-light illumination room temperature HCHO gas-sensing mechanism of ZnO with different

- nanostructures. *Sensors and Actuators B: Chemical*, 227, 220-226.
- Drmosh, Q. A., Alade, I. O., Qamar, M., & Akabar, S. (2021). Zinc oxide-based acetone gas sensors for breath analysis: A review. *Chemistry: An Asian Journal*, 16(12), 1519-1538.
- Hassan, M. M., Khan, W., Naqvi, A. H., Mishra, P., & Islam, S. S. (2014). Fe dopants enhancing ethanol sensitivity of ZnO thin film deposited by RF magnetron sputtering. *Journal of Materials Science*, 49, 6248-6256.
- Hongsith, N., Wongrat, E., Kerdcharoen, T., & Choopun, S. (2010). Sensor response formula for sensor based on ZnO nanostructures. *Sensors and Actuators B: Chemical*, 144, 67-72.
- Hosseini, Z.S., Irajzad A., & Mortezaali, A. (2015). Room temperature H<sub>2</sub>S gas sensor based on rather aligned ZnO nanorods with flower-like structures. *Sensor and Actuators B: Chemical*, 207, 865-871.
- Joshi, L. P., Khatri, B. V., Gyawali, S., Gajurel, S., & Chaudhary, D. K. (2021). Green Synthesis of Zinc Oxide Nanoparticles Using Ixora Coccinea Leaf Extract for Ethanol Vapour Sensing. *Journal of Physical Science*, 32(2), 15-26.
- Kashout, A. B., Soliman, H. M. A., Hassan, H. S., & Aousehly, A. M. (2010). Fabrication of ZnO and ZnO:Sb nanoparticles for gas sensor applications, *Journal of Nanomaterials*, 2010.
- Khayatian, A., Kashi, M. A., Azimirad, R., & Safa, S. (2014). Enhanced gas-sensing properties of ZnO nanorods encapsulated in an Fe-doped ZnO shell. *Journal of Physics D: Applied Physics*, 47, 075003.
- Kishore, K. R., Balamurugan, D., & Jeypakash, B. G. (2021). CuO nanograins: synthesis and acetone vapour detection. *Journal of Materials Science: Materials in Electronics*, 32, 1204-1220.
- Li, W. Q., Ma, S. Y., Luo, J., Mao, Y. Z., Cheng, L., Gengzang, D. J., Xu, X. L., & Yan, S. H. (2014). Synthesis of hollow SnO<sub>2</sub> nanobelts and their application in acetone sensor, *Materials Letters*, 132, 338-341.
- Prajapati, C. S., & Sahay, P. P. (2013). Influence of In doping on the structural, optical and acetone sensing properties of ZnO nanoparticulate thin films. *Materials science in semiconductor processing*, 16, 200-210.
- Qi, Q., Zhang, T., Liu, L., Zheng, X., Yu, Q., Zeng, Y., & Yang, H. (2008). Selective acetone sensor based on dumbbell-like ZnO with rapid response and recovery. *Sensors and Actuators B: Chemical*, 134, 166-170.
- Qiang, Z., Ma, S. Y., Jiao, H. Y., Jin, W. X., Wang, T. T., Jiang, X. H., & Zhang, Z. Y. (2016). Solvothermal synthesis of 3D leaf-like  $\alpha$ -Fe<sub>2</sub>O<sub>3</sub> and its gas-sensing properties research. *Materials Letters*, 181, 29-33.
- Samanta, P., Bagchi, S., & Mishra, S. (2015). Synthesis and Sensing characterization of ZnO nanofibers prepared by Electrospinning. *Materials Today: Proceedings*, 2(9), 4499-4502.
- Sirdeshpande, K. D., Sridhar, A., Cholkar, K. M., & Selvaraj, R. (2018). Structural characterization of mesoporous magnetite nanoparticles synthesized using the leaf extract of Calliandra haematocephala and their photocatalytic degradation of malachite green dye. *Applied Nanoscience*, 8(4), 675-683.
- Tang, H., Li, Y., Zheng, C., Ye, J., Hou, X., & Lv, Y. (2007). An ethanol sensor based on cataluminescence on ZnO nanoparticles. *Talanta*, 72(4), 1593-1597.
- Wang, Y., Meng, X. N., & Cao, J. L. (2020). Rapid detection of low concentration CO using Pt-loaded ZnO nanosheets. *Journal of hazardous materials*, 381, 120944.
- Wang, L., Teleki, A., Pratsinis, S. E., & Gouma, P. I. (2008). Ferroelectric WO<sub>3</sub> nanoparticles for acetone selective detection. *Chemistry of Materials*, 20(15), 4794-4796.
- Wongrat, E., Chanlek, N., Chueaiarrom, C., Thupthimchun, W., Samransuksamer, B., & Choopun, S. (2017). Acetone gas sensors based on ZnO nanostructures decorated with Pt and Nb. *Ceramics International*, 43, S557-S566.
- Xi, Y., Hu, C. G., Han, X. Y., Xiong, Y. F., Gao, P. X., & Liu, G. B. (2007). Hydrothermal synthesis of ZnO nanobelts and gas sensitivity property. *Solid state communications*, 141(9), 506-509.
- Xiao, Y., Lu, L., Zhang, A., Zhang, Y., Sun, L., Huo, L., & Li, F. (2012). Highly enhanced acetone sensing performances of porous and single crystalline ZnO nanosheets: high percentage of exposed (100) facets working together with surface modification with Pd nanoparticles. *ACS applied materials & interfaces*, 4(8), 3797-3804.
- Xu, X. L., Chen, Y., Ma, S. Y., Li, W. Q., & Mao, Y. Z. (2015). Excellent acetone sensor of La-doped ZnO nanofibers with unique bead-like structures. *Sensors and Actuators B: Chemical*, 213, 222-233.
- Zeng, Y., Zhang, T., Yuan, M., Kang, M., Lu, G., Wang, R., Fan, H., He, Y., & Yang, H. (2009). Growth and selective acetone detection based on ZnO nanorod arrays. *Sensors and Actuators B: Chemical*, 143(1), 93-98.
- Zhang, Y., Ram, M. K., Stefanakos, E. K., & Goswami, D. Y. (2012). Synthesis, characterization, and applications of ZnO nanowires. *Journal of Nanomaterials*, 2012, 1-22.
- Zhang, Y. H., Liu, C. Y., Jiu, B. B., Liu, Y., & Gong, F. L. (2018). Facile synthesis of Pd-decorated ZnO nanoparticles for acetone sensors with enhanced performance. *Research on Chemical Intermediates*, 44(3), 1569-1578.
- Zhao, G., Xuan, J., Liu, X., Jia, F., Sun, Y., Sun, M., Yin, G., & Liu, B. (2019). Low-cost and high-performance ZnO nanoclusters gas sensor based on new-type FTO electrode for the low-concentration H<sub>2</sub>S gas detection. *Nanomaterials*, 9, 435-445.
- Zhu, L., & Zeng, W. (2017). Room-temperature gas sensing of ZnO-based gas sensor: A review. *Sensors and Actuators A: Physical*, 267, 242-261.